Alexandria Engineering Journal (2019) 58, 603–610

HOSTED BY

Alexandria University

Alexandria Engineering Journal

www.elsevier.com/locate/aej
www.sciencedirect.com

ORIGINAL ARTICLE

Infrared thermography applied to the prediction of structural vibration behaviour

Stephen M. Talai [a,*], Dawood A. Desai [a], P. Stephan Heyns [b]

[a] Sound & Vibration Group, Tshwane University of Technology, Private Bag X680, Pretoria 0001, South Africa
[b] Centre for Asset Integrity Management, University of Pretoria, Private Bag X20, Hatfield 0028, South Africa

Received 29 November 2016; revised 19 July 2017; accepted 3 March 2019
Available online 18 June 2019

KEYWORDS

Structural health monitoring;
Frictional temperature evolution;
Online monitoring;
Thermal imaging

Abstract This paper concerns the development of methodology for use of Infrared thermography (IRT) for online prediction of mechanical structural vibration behaviour; given that it has extensively been applied in non-destructive technique for evaluation of surface cracks through the observation of thermal imaging of the vibration-induced crack heat generation. To achieve this, AISI 304 steel cantilever beam coupled with a slipping friction rod was subjected to a forced excitations with an infrared camera capturing the thermal profile at the friction interface. The analysis of thermal image data recorded (radiometric) for the frictional temperature time domain waveform using a MATLAB FFT algorithm in conjunction to IR camera frequency resolution of 120 Hz and the use of the heat conduction equation with the help of a finite difference approach successfully identified the structural vibration characteristics in terms of frequency and displacement, the maximum relative errors being 0.09% and 5.85% for frequencies and displacements, respectively. These findings are particularly useful in overcoming many limitations inherent in some of the current vibration measuring techniques in harsh and remote environments.

1. Introduction

The structural integrity of mechanical dynamic structures is key to its successful operation [1–3]. The available literature indicates that, condition monitoring of vibrating structures has long been an active area of research since 1950s; when Arthur Crawford first acknowledged the challenge to acquire an effective way for structural vibration analysis. Le et al. [4] contends that in today's mechanical and aerospace engineering communities, need for enhanced ability to monitor dynamic structures and detect the potential damages at the earliest possible stage for effective structural health monitoring (SHM) is ever increasing.

For decades, however, vibration monitoring has been utilised to assess SHM in predicting potential failures that, in turn, enhance the reliability and availability [2,5]. The direct methods of measurements such as strain gauges have predominantly been used. Although they have the advantage of performing measurement of an individual structure, it has several disadvantages such as; shorter sensor life span due to continued cyclic loading; leading to failures by fatigue [6]. Laser Doppler vibrometry with an Eulerian approach allows overcoming most of the limitations mentioned in the use of

* Corresponding author.
E-mail address: TalaiSM@tut.ac.za (S.M. Talai).
Peer review under responsibility of Faculty of Engineering, Alexandria University.

https://doi.org/10.1016/j.aej.2019.03.008

strain gauges. Nevertheless, Castellini et al. [7] reported that its main limitations are speckle effects and poor signal-to-noise ratio when measuring vibration on the low diffusive surface. Likewise, Interferometry method has the ability to provide traceability of vibration frequency measurement as it relates directly to the definition of the meter. Its measurement accuracy, however, is limited by the environment [8], thus, not be possible to perform the vibration measurement in a turbulent environment for instance power plants.

Interestingly, infrared thermography (IRT) has been greatly applied to vibrothermography non-destructive technique where the surface cracks are evaluated through the observation of thermal imaging of vibration-induced heat generation. Recent studies have shown that defect heating in cracked metallic structure is primarily generated by frictional rubbing on crack faces [9]. Mabrouki et al. [10] investigated the vibrothermography for detection of fatigue cracks in steel compact tension specimen. Lahiri et al. [11] proposed the active IRT based technique for detecting defects in ferromagnetic specimens using low frequency alternating magnetic field induced heating. The authors observed an increase in the surface temperature using an infrared camera due to induced eddy current leading to joules heating. Furthermore, Montanini and Freni [12] established that there exists a correlation of vibration characteristics to viscoelastic heat generation in vibrothermography.

Conversely, friction is often considered by engineers as detrimental to the design of dynamic mechanisms involving mating parts. However, it has long been established that it can as well provide a very effective means of dissipating vibratory energy in elastic structures. This technique is in applications such as turbomachinery bladed disks [2,13], where either the lacing wire is incorporated at the chosen location of the blade structure or direct interaction of the constitutive blades through shrouded tip approach for enhancing passive dissipation of vibratory energy. In reality, it is often structural joints that are more responsible for energy dissipation than the (solid) material itself [14,15]. Ultimately, this leads to temperature increase at the contact interface [16]. Therefore, the analysis of frictional heat generation due to interacting components can result to a quick and reliable indication of the structural vibration characteristics.

A typical industrial application of IRT based condition monitoring on a dynamic mechanical component *(compressor motor)* including its thermal image is presented in Fig. 1, where abnormal surface temperature in an indication of probable flaw. Accordingly, despite the large amount of research conducted on condition monitoring using IRT as indicated in the recent comprehensive literature review by Bagavathiappan et al. [17], little attention has been paid to vibration measurement. Interestingly, Dimarogonas and Syrimbeis [18] successfully studied the vibration modes from thermal signature of a vibrating plate due to material damping. To date, however, the concept has not been explored even though IRT has matured and widely accepted as a condition monitoring tool where temperature is measured in a non-contact manner.

Consequently, it is important to mention that friction is a complex phenomenon due to its nonlinearity [19]. The difficulty, however, lies in relating frictional temperature time domain waveform to vibration behaviour. Therefore, it was the aim of this study to develop a practical methodology. In order to achieve this, AISI 304 cantilever beam coupled with slipping friction rod was subjected to a forced excitations with an infrared camera capturing the thermal profile at the friction interface concurrently. An electrodynamic shaker attached to the beam end vie stinger provided the excitation. Also, an accelerometers was attached to the beam for acquiring the actual beam displacement for the intention of validating the parameters predicted using IRT. The methodology developed forms the basis for online SHM employing IRT which is of great beneficial to the maintenance, most importantly, in harsh and turbulent environment applications.

2. Mathematical model

2.1. Structural vibration frequencies

The post analysis of thermal imaging data yields the temperature time-domain waveform. It does not seem, by eye, to have

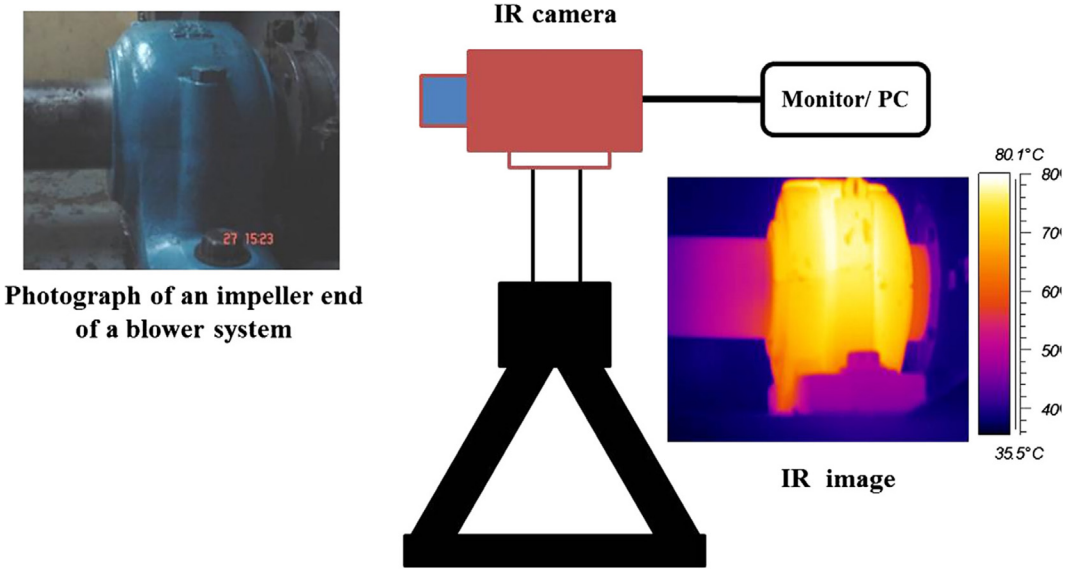

Fig. 1 A typical practical setup for temperature based condition monitoring using IRT [17].

any underlying sinusoidal signal components, instead it's completely random and consists of noise. However, the Discrete Fourier Transform (DFT) analysis is utilised to check for the spectral peak. The MATLAB Fast Fourier Transform (FFT) function performs computation of DFT in an efficient way. Therefore, considering the sampling frequency of an IR camera being used for SHM, and the frictional temperature time-domain waveform, the structural vibration frequency is evaluated.

2.2. Correlation of beam transverse displacements to surface frictional temperature distribution

The heat conduction equation for the Cartesian co-ordinate system (x, y, z) on the beam surface differential element can be expressed as [20]

$$\frac{\partial^2\theta}{\partial x^2}+\frac{\partial^2\theta}{\partial y^2}+\frac{\partial^2\theta}{\partial z^2}+\frac{q_g}{k}=\frac{\rho c}{k}\frac{\partial\theta}{\partial t} \tag{1}$$

where θ is the temperature rise on the beam surface, k is thermal conductivity, ρ is the material density and c is the specific heat capacity and q_g is the heat generated per unit volume. Making the following assumptions:

i. Temperature has reached a steady state condition, hence, $\frac{\partial\theta}{\partial t}=0$.
ii. The beam is thin, hence, the temperature distribution is uniform along the thickness. Therefore, $\frac{\partial^2\theta}{\partial z^2}=0$.
iii. Heat lost through forced convection is 30 W/m^2 K at 22 °C [21]. It obeys the Newton's law of cooling $\left(q=\frac{h_{con}}{ck}\theta\right)$ and is the heat lost on both sides of the beam. However, heat lost by radiation is ignored since its negligible compared to the heat lost through forced convection [18].

Hence, the heat conduction Eq. (1) becomes,

$$\frac{\partial^2\theta}{\partial x^2}+\frac{\partial^2\theta}{\partial y^2}+\frac{q_g}{k}-\frac{2h_{con}}{ck}\theta=0 \tag{2}$$

By analysing the beam surface temperature using the grid distribution technique given in Fig. 2, the temperature rise finite difference equations for the grid in Δx and Δy are

$$\frac{\partial^2\theta}{\partial x^2}=\frac{1}{(\Delta x)^2}\left(\theta_{i+1}-2\theta_{i,j}+\theta_{i-1}\right),$$
$$\frac{\partial^2\theta}{\partial y^2}=\frac{1}{(\Delta y)^2}\left(\theta_{j+1}-2\theta_{i,j}+\theta_{j-1}\right) \tag{3}$$

Substituting Eq. (3) into Eq. (2) and rearranging, the heat distribution in terms of temperature finite differences developed

$$q_g(x,y)=k\left[\frac{2h_{con}}{ck}\theta_{i,j}-\frac{\partial^2\theta}{\partial x^2}-\frac{\partial^2\theta}{\partial y^2}\right] \tag{4}$$

Considering the beam with frictional interface that is excited by a sinusoidal force as shown in Fig. 3, the steady state displacement response can be given by [22]

$$z(t)=Z\sin(\omega t) \tag{5}$$

where $z(t)$ is the displacement at time t, Z is the amplitude and ω is the excitation frequency. The frictional heat generation,q_g per half a cycle is given by [23]

$$q_g=2\mu F_{CR}fZ \tag{6}$$

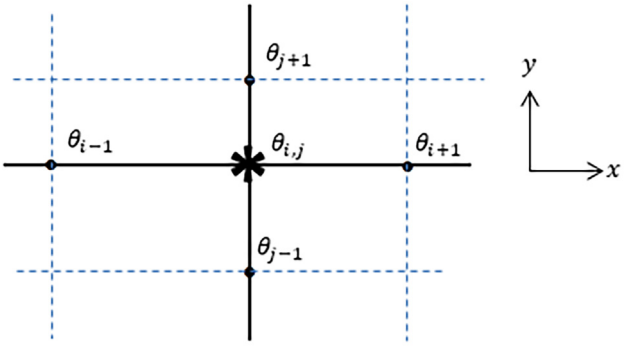

Fig. 2 Finite surface temperature distribution grid.

Table 1 Beam and friction rod geometric dimensions.

Description	Parameters
Beam mass	0.10 kg
Length	300 mm
Width	25 mm
Thickness	2 mm
Lacing wire (friction rod) diameter	5 mm
Beam hole diameter [tolerance grade: *F*8/*js*7] [24]	$5^{+0.422}_{+0.412}$ mm
Beam-lacing wire hole location from the fixed end	250 mm
Exciters location from the fixed end	290 mm

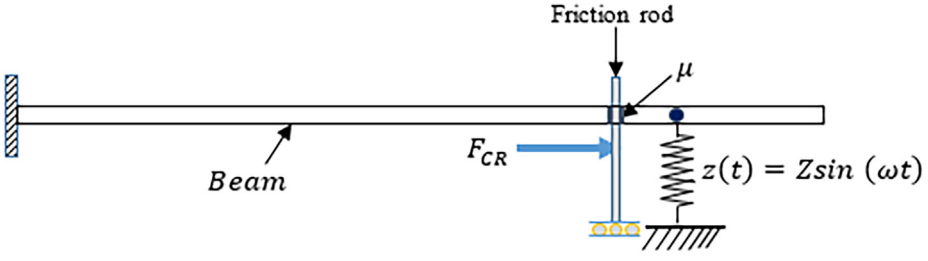

Fig. 3 Beam frictional heat generation.

Table 2 AISI 304 material properties [25].

Structural properties	Parameters
Density, ρ	7740 kg/m^3
Young modulus, E	200 GPa
Poisson ratio, v	0.33
Static friction coefficient, μ_s ($\mu_k = 0.75\mu_s$) [26]	0.15
Thermal properties	
Thermal conductivity, k	16.5 W/m K
Specific heat capacity, c	500 J/kg K

where μ coefficient of friction, F_{CR} is the contact resultant force, f excitation frequency, hence, substituting Eq. (5) into Eq. (6)

$$q_g = \frac{2\mu F_{CR} f z(t)}{sin(\omega t)} \tag{7}$$

In order to obtain the beam displacement equation from the acquired thermal imager, the surface temperature is equated to the frictional heat evaluation. Hence, comparing Eqs. (4) and (7), the equation of beam transverse displacement is developed

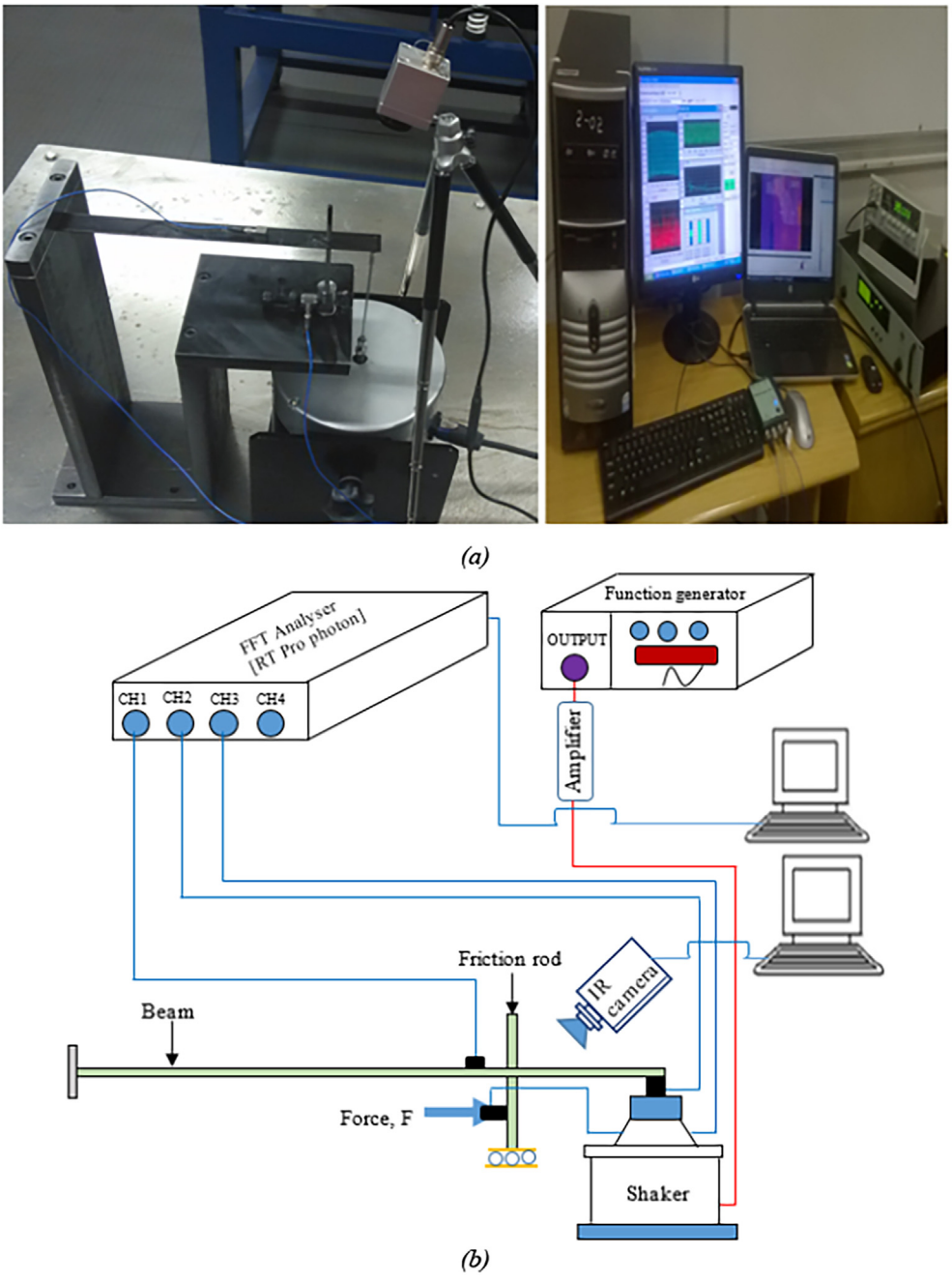

Fig. 4 Frictional temperature evolution monitoring *(a) Laboratory experimental setup (b) schematic representation.*

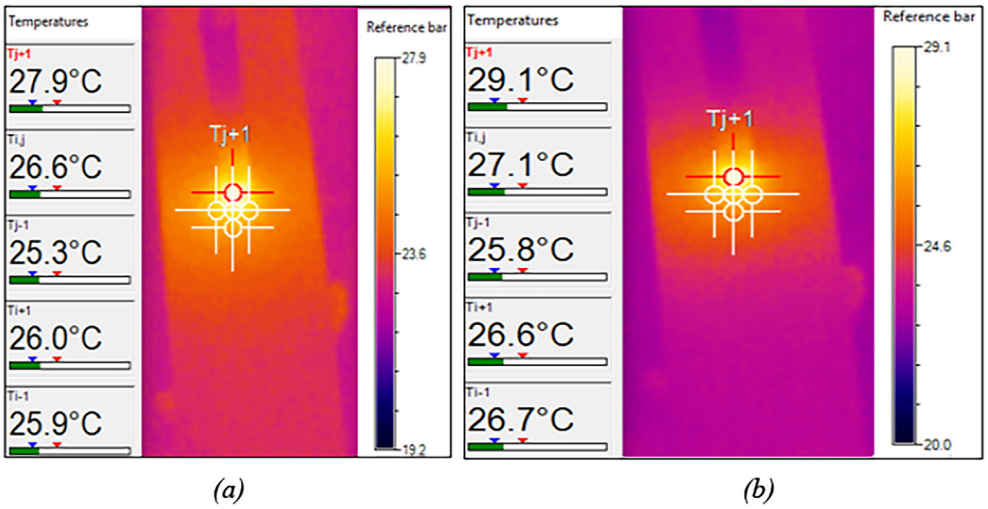

Fig. 5 IR thermal images for shaker forcing frequency *(a) 20 and (b) 50* Hz.

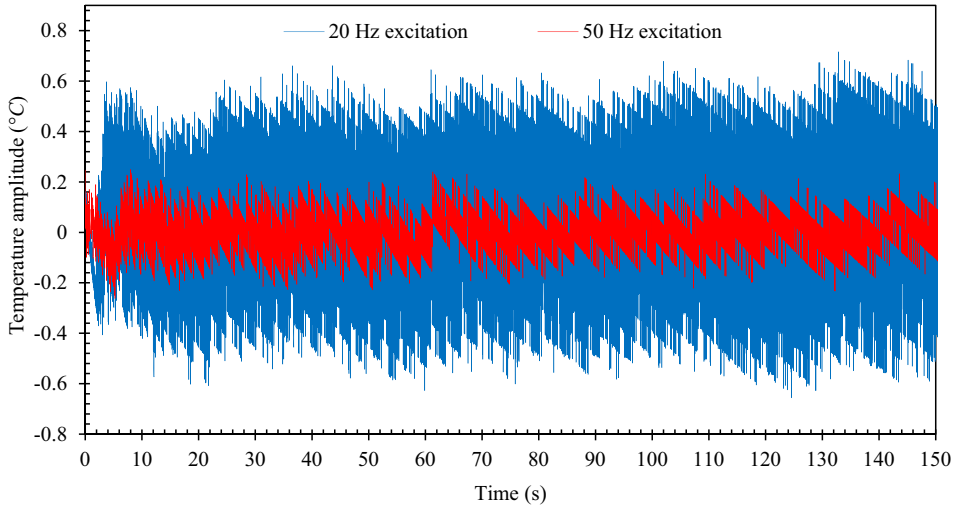

Fig. 6 Frictional temperature evolution.

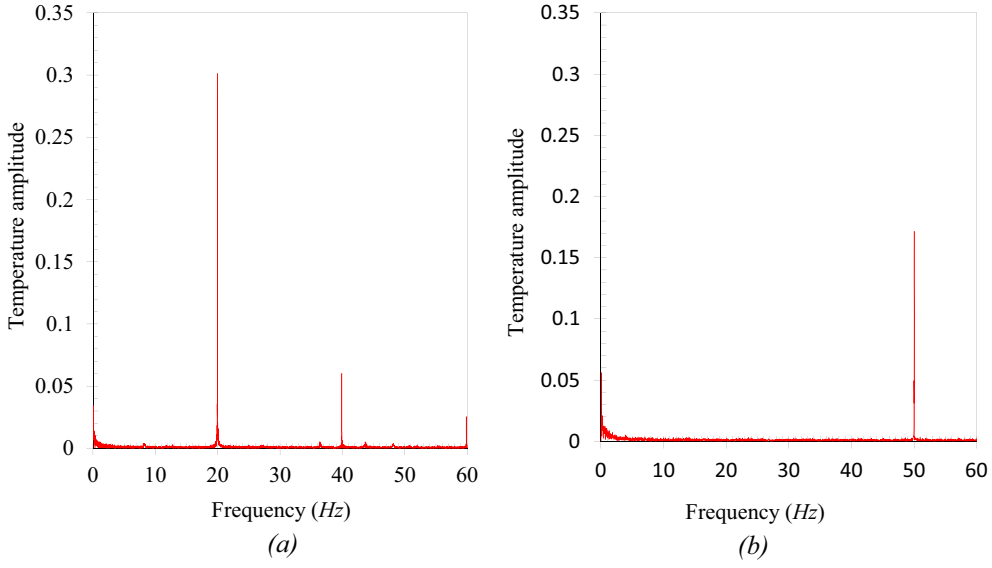

Fig. 7 FFT of temperature evolution for beam excitation frequencies *(a)* at 20 Hz *and (b) at* 50 Hz.

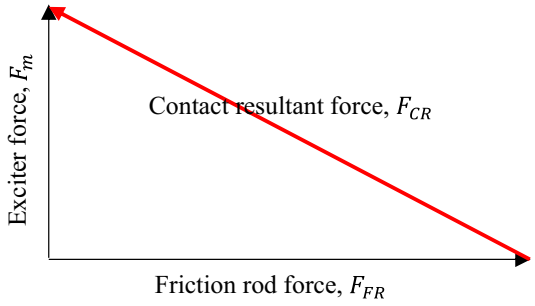

Fig. 8 Beam-friction rod interface force components.

$$z(t) = \frac{k \sin(\omega t)}{2\mu F_{CR}\omega}\left[\frac{2h_{con}}{ck}\theta_{i,j} - \frac{\partial^2\theta}{\partial x^2} - \frac{\partial^2\theta}{\partial y^2}\right] \quad (8)$$

Eq. (8) allows the computation of the beam transverse displacement from the analysis of the thermal imager surface temperature distribution.

3. Materials and experimental method

3.1. Materials

Both the beam and the friction rod were manufactured of AISI 304 stainless steel due to its low thermal conductivity, hence, generate heat with any slight frictional effect [10]. The geometric and material properties are given in Tables 1 and 2, respectively.

3.2. Experimental procedure

The laboratory experimental setup was as presented in Fig. 4.

Initially, the pre-load force of 2.25 N was applied to the friction rod for the purpose of uniformity. This was achieved by tightening the adjusting bolt that pushed the friction rod laterally via a sleeve, while a PCB force transducer model 208C02 with sensitivity rating of 11.24 mV/N measured the attained force. The forcing frequency signals obtained from the function generator (FG-7005C) were amplified *(power amplifier model: LA-1500)* before being transmitted to the electrodynamic exciter *(Type: 4824, Brüel & Kjær)* to facilitate the beam forced excitation via a stinger coupled with a PCB force transducer model 208C04 with sensitivity rating of 1.124 mV/N, hence, measure the output force. The forced excitation frequencies considered were 20 Hz and 50 Hz. These were considered based on Shannon's sampling rate theorem of 0.4 times the rated optical frequency resolution of the IR camera used in this study. Concurrently, a Micro-epsilon (TIM160) infrared camera was focused on the beam-friction rod interface to capture the thermal image. The properties of the IR camera used are: thermal sensitivity of 0.08 K, spectral range of 7.5–13 μm, optical resolution of 160 × 120 pixels, optical frequency resolution of 120 Hz.

The beam displacement response was measured using a miniature Deltatron accelerometer type 4507 with sensitivity rating of 97.96 mV/g and mass of 4.8 g (Brüel & Kjær) that was mounted to the surface using beeswax. On the other hand, the RT pro-Photon FFT analyser (*Brüel & Kjær*) acquired the dynamic measurements. The problem of low thermal emissivity of the beam surface was eliminated by applying black paint which is consistent with the standard practice in this field [10].

4. Results and discussions

During the experimental period, the ambient room temperatures recorded was 22.4 °C. The thermal imaging considered 150 s recording time as required by the operation manual for the reliable real time temperature recording *(full pixel recording)*. This short time duration goes a long way in avoiding the effect of significant wear rate at the friction interface during excitation. The acquired images with the grid interface temperature distributions emanating from excitation frequencies considered are shown in Fig. 5, while the MATLAB detrended frictional temperature evolution time domain corresponding to the hottest interface in Fig. 6. As expected, the structure under higher excitation frequency allows the frictional interface to slide against each other more times; unlike at lower frequencies leading to greater frictional heat generation as seen with a temperature difference of 1.2 °C among the images (Fig. 5).

The MATLAB FFT algorithm was utilised to transform the detrended frictional temperature evolution time history (Fig. 6) into the frequency domain (Fig. 7). The structural vibration frequencies corresponds to the longest peak of the spectrum, hence, extracted as 20.0059 Hz (Fig. 7a) and 50.0015 Hz (Fig. 7b) for the beam forcing frequencies of 20 and 50 Hz, respectively. The interfaces contact resultant forces were computed based on the representation given in Fig. 8. where $F_{CR} = \sqrt{\left(F_m{}^2 + F_{FRP}{}^2\right)}$, F_m is the maximum exciter force and P_{FRP} is the friction rod pre-load force. Therefore, utilising this expression, the interface frictional force corresponding to the excitation frequencies of 20 Hz and 50 Hz were 5.974 N and 6.826 N, respectively. The beam displacements were analysed using the finite element approach proposed in Fig. 2 in conjunction to interfacial temperature distribution in Fig. 5. In the case of 20 Hz (Fig. 5a), the finite nodal temperature using Eq. (3) along X and Y directions were -1.3 Â°C/mm^2 and 0.00 Â°C/mm^2, respectively. From Eq. (8), the IRT predicted displacement obtained as 2.239 mm. Similarly, in the case of 50 Hz (Fig. 5b), finite nodal temperature along X and Y directions were -0.9 Â°C/mm^2 and 0.7 Â°C/mm^2, respectively; while the displacement using Eq. (8) was obtained as 0.877 mm. The higher displacement at 20 Hz compared to at 50 Hz justifies the larger temperature range variation for the former than the latter as depicted in Fig. 6.

On the other hand the frequency responses acquired using the described accelerometer presented in Fig. 9, extracted the beam vibration frequencies as 20.0196 Hz and 50.049 Hz for 20 Hz and 50 Hz forcing frequencies, respectively. Interestingly, these compared quite well with those acquired using IRT approach with a relative errors being 0.07% and 0.09% for the former and latter, respectively.

Further, the beam displacement spatial statistics was as shown in Table 3, the mean being 2.108 mm and 0.912 mm for the forcing frequencies of 20 Hz and 50 Hz, respectively. This exhibited relative errors of 5.85% and 3.98% for the former and latter. The errors were attributed to partly location of accelerometer being towards the beam fixed end and use

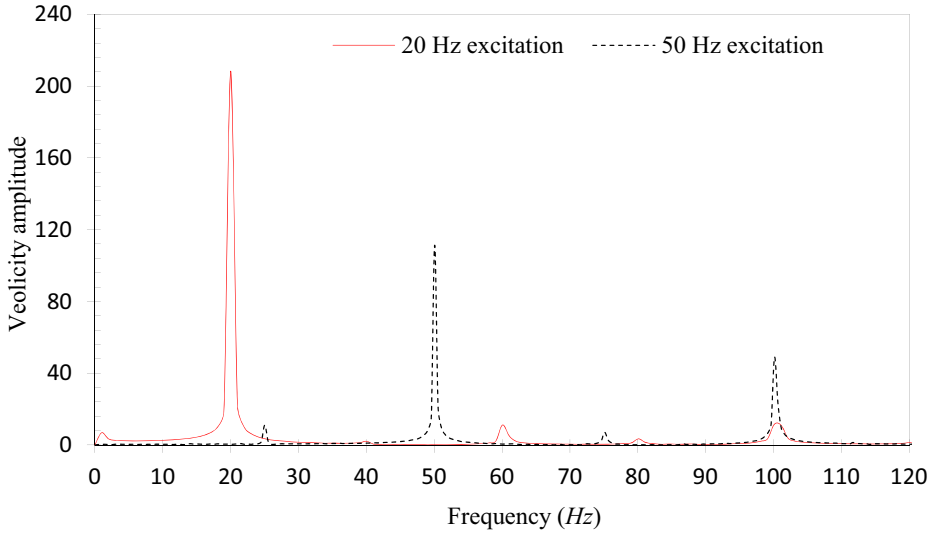

Fig. 9 Beam FFT of velocity response.

Table 3 Accelerometer measured displacement statistics.

	Beam displacement (mm)	
Description	20 Hz forcing frequency	50 Hz forcing frequency
Mean	2.108	0.912
Max	6.303	2.002
Min	0.010	0.025
Range	6.293	1.977
Std. deviation	2.015	0.619

of coefficient of frictional as well as convective heat losses from the literature that may not be the real values as per the experimental setup.

5. Conclusion

In this paper, the adequacy of monitoring the mechanical structural vibration behaviour in terms of frequency and displacement, based on a simple cantilever beam coupled with a friction interface using IRT has been examined practically. The good agreement exhibited by IRT and accelerometer measured dynamic parameters was an evidence of suitability of IRT developed methodology in application to mechanical structural vibration characteristics prediction, most importantly, the vibration frequency since friction coefficient cannot be obtained quickly online. Moreover, the frictional thermal distribution showed to be non-linear in nature and the equations of finite difference grid can be used in computation of the structural displacement from the thermal imager. The findings of this study has a great significance to the mechanical and aerospace engineering communities for the effective SHM of dynamic structures online using infrared thermography, thus, reducing the downtime and maintenance cost, leading to increased efficiency.

Conflict of interest

There exist no conflict of interest.

Acknowledgement

The authors greatly appreciate the support of Eskom Power Plant Engineering Institute (South Africa), University of Pretoria and Tshwane University of Technology for funding this research.

References

[1] F. Wei, Q. Pizhong, Vibration-based damage identification methods: a review and comparative study, Struct. Health Monit. 10 (1) (2010) 83–111.
[2] N.K. Mukhopadhyay, S.G. Chowdhury, G. Das, I. Chattoraj, S.K. Das, D.K. Bhattacharya, An investigation of the failure of low pressure steam turbine blades, Eng. Fail. Anal. 5 (3) (1998) 181–193.
[3] S.E. Moussavi Torshizi, S.M. Yadavar Nikravesh, A. Jahangiri, Failure analysis of gas turbine generator cooling fan blades, Eng. Fail. Anal. 16 (5) (2009) 1686–1695.
[4] T.T.H. Le, N. Point, P. Argoul, G. Cumunel, Structural changes assessment in axial stressed beams through frequencies variation, Int. J. Mech. Sci. 110 (2016) 41–52.
[5] S.J. Rao, Turbo-Machine Blade Vibration, first ed., New Age International Publishers, New Delhi, 1991, pp. 7–20.
[6] B.O. Al-Bedoor, Discussion of the available methods for blade vibration measurement, in: ASME 2002 Pressure Vessels and Piping Conference. Vancouver, BC: Canada, 1561, 2002, pp. 53–61.
[7] P. Castellini, M. Martarelli, E.P. Tomasini, Laser Doppler Vibrometry: development of advanced solutions answering to technology's needs, Mech. Syst. Sig. Process. 20 (2006) 1265–1285.
[8] N. Brock, J. Hayes, B. Kimbrough, J. Millerd, M. North-Morris, M. Novak, C.J. Wyan, Dynamic interferometry, in: Proceedings of SPIE 5875, 2005.
[9] J. Renshaw, J.C. Chen, S.D. Holland, T.R. Bruce, The sources of heat generation in vibrothermography, NDT E Int. 44 (8) (2011) 736–739.
[10] F. Mabrouki, M. Thomas, M. Genest, A. Fahr, Frictional heating model for efficient use of vibrothermography, NDT E Int. 42 (5) (2009) 345–352.

[11] B.B. Lahiri, S. Bagavathiappan, C.C. Soumya, V. Mahendran, V.P.M. Pillai, J.P.J. T. Jayakumar, Infrared thermography based defect detection in ferromagnetic specimens using a low frequency alternating magnetic field, Infrared Phys. Technol. 64 (2014) 125–133.
[12] R. Montanini, F. Freni, Correlation between vibrational mode shapes and viscoelastic heat generation in vibrothermography, Ndt E International 58 (2013) 43–48.
[13] M. Singh, G. Lucas, Blade Design & Analysis for Steam Turbines, The McGraw-Hill Companies, United States of America, 2011, pp. 20–60.
[14] A. Guran, F. Pfeiffer, K. Popp, Dynamics with Friction Modelling, Analysis and Experiments, World Scientific, Singapore, 2001, pp. 20–21.
[15] G. Straffelini, Friction and Wear: *Methologies for Design and Control*, Springer, Trento, 2015, pp. 21–58.
[16] A.D. Dimarogonas, S.A. Paipetis, T.G. Chondros, Analytical Methods in Rotor Dynamics (second edition) New York London, Springer Dordrecht Heidelberg, 2013, pp. 203–263.
[17] S. Bagavathiappan, B.B. Lahiri, T. Saravanan, J. Philip, T. Jayakumar, Infrared thermography for condition monitoring – a review, Infrared Phys. Technol. 60 (2013) 35–55.
[18] A.D. Dimarogonas, N.B. Syrimbeis, Thermal signatures of vibrating rectangular plates, J. Sound Vib. 157 (3) (1992) 467–476.
[19] D. Thorby, Structural Dynamics and Vibration in Practice: An Engineering Handbook, Elsevier Science, London, 2008, pp. 23–30.
[20] R.K. Rajput, in: Heat and Mass Transfer, S. Chard & Company Ltd, 2006, pp. 30–40.
[21] S.F. Miller, A.J. Shih, Thermo-mechanical finite element modeling of the friction drilling process, J. Manuf. Sci. Eng. 129 (2007) 531–538.
[22] C.F. Beards, Structural Vibration: Analysis and Damping, Elsevier Science, London, 2003, pp. 200–210.
[23] S.S. Rao, Mechanical Vibrations, fifth ed., Prentice Hall: Pearson Education, 2011, pp. 293–294.
[24] W.P. Sanders, in: Turbine Steam Path Engineering for Operations and Maintenance Staff, first ed., Richmond Hill, Ontario: Canada, 1996, pp. 236–239.
[25] C.V. Madhusudana, Thermal conductance of cylindrical joints, Int. J. Heat Mass Transf. 42 (1999) 1273–1287.
[26] J.T. Oden, J.A. Martins, Models and computational methods for dynamic friction phenomena, Comput. Methods Appl. Mech. Eng. 52 (1985) 527–634.